Mon. Not. R. Astron. Soc. **346,** 689–703 (2003)

Multiwavelength observations revealing the evolution of the outburst of the black hole XTE J1118+480

S. Chaty,[1,2,3★] C. A. Haswell,[3] J. Malzac,[4,5] R. I. Hynes,[6,7] C. R. Shrader[8] and W. Cui[9]

[1]*Université Paris 7, Fédération APC, 2 place Jussieu, 75005 Paris, France*
[2]*Service d'Astrophysique, DSM/DAPNIA/SAp, CEA-Saclay, Bat. 709, L'Orme des Merisiers F-91 191 Gif-sur-Yvette Cedex, France*
[3]*Department of Physics and Astronomy, The Open University, Walton Hall, Milton Keynes MK7 6AA*
[4]*Institute of Astronomy, Madingley Road, Cambridge CB3 0HA*
[5]*Osservatorio Astronomico di Brera, Via Brera, 28, 20121 Milano, Italy*
[6]*Astronomy department, The University of Texas at Austin, 1 University Station C1400, Austin, TX 78712-0259, USA*
[7]*Department of Physics and Astronomy, University of Southampton, Southampton SO17 1BJ*
[8]*Laboratory for High-Energy Astrophysics, NASA Goddard Space Flight Centre, Greenbelt, MD 20771, USA*
[9]*Department of Physics, Purdue University, 1396 Physics Building, West Lafayette, IN 47907-1396, USA*

Accepted 2003 August 12. Received 2003 July 10; in original form 2002 August 30

ABSTRACT

We report multiwavelength observations of the soft X-ray transient XTE J1118+480, which we observed with UKIRT, *Hubble Space Telescope* (*HST*), *RXTE*, *Extreme Ultraviolet Explorer* (*EUVE*) and many other instruments and facilities. Adding radio (Ryle Telescope, VLA), submillimetre (JCMT) and X-ray (*Chandra* and *SAX*) data from the literature, we assembled the most complete spectral energy distribution (SED) of this source yet published. We followed the evolution of this source for 1 yr, including six observations performed during the outburst, and one observation at the end of the outburst. Because of the unusually high galactic latitude of XTE J1118+480, it suffers from very low extinction, and its SED is nearly complete, including extreme ultraviolet observations. XTE J1118+480 exhibits an unusually low low/hard state (estimated inner radius of $350R_{\rm s}$) and a strong non-thermal contribution in the radio to optical domain, which is likely to be due to synchrotron emission. We discuss the interstellar column density and show that it is low, between 0.80 and 1.30×10^{20} cm^{-2}. We analyse the evolution of the SED during the outburst, including the contributions from the companion star, the accretion disc, the outflow, and relating irradiation and variability of the source in different bands to the SED. We find no significant spectral variability during the outburst evolution, consistent with the presence of a steady outflow. An analysis of its outflow to accretion energy ratio suggests that the microquasar XTE J1118+480 is analogous to radio-quiet quasars. This, combined with the inverted spectrum from radio to optical, makes XTE J1118+480 very similar to other microquasar sources, e.g. GRS 1915+105 and GX 339−4 in their low/hard state. We model the high-energy emission with a hot disc model, and discuss different accretion models for the broad-band spectrum of XTE J1118+480.

Key words: accretion, accretion discs – stars: individual: XTE J1118+480 – dust, extinction – infrared: stars – ultraviolet: stars – X-rays: binaries.

1 INTRODUCTION

Soft X-ray transients (SXTs), also called X-ray novae, are a class of low-mass X-ray binaries (LMXBs). Among this class of sources, more than 70 per cent are thought to contain black holes (Charles 1998). The compact object accretes matter through an accretion disc from a low-mass star via Roche lobe overflow. The history of these sources is characterized by long periods of quiescence, typically lasting decades, punctuated by very dramatic outbursts. SXTs are usually discovered in X-rays, but outbursts are visible at every wavelength and, in particular, are often accompanied by radio activity. A typical outburst is characterized by soft X-ray emission dominated by thermal emission from the hot inner accretion disc, and optical/ultraviolet (UV) emission produced by reprocessing of X-rays.

★E-mail: chaty@cea.fr

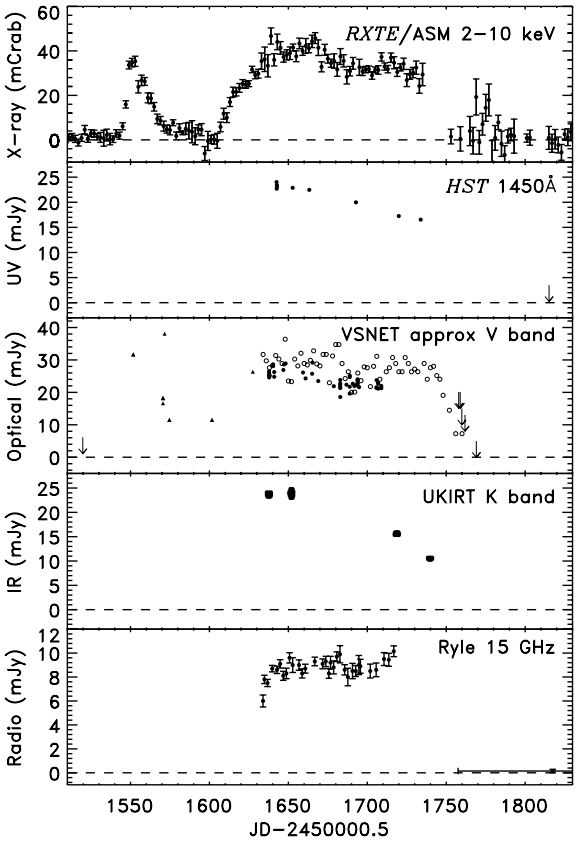

Figure 1. Multiwavelength light curve of XTE J1118+480 in 2000: the six epochs of our observations are indicated by the *HST* points. The top panel shows *RXTE/ASM* 2–10 keV count rates in 2-d averages. Periods with too few dwells for a precise measurement have been excluded for clarity. The second panel is *HST*/STIS far-UV fluxes derived from E140M spectroscopy and an upper limit from the late G140L observation. The middle panel shows VSNET optical measurements (http://www.kusastro.kyoto-u.ac.jp/vsnet/Summary/j1118.html). Open circles are 2-d averages of visual estimates. Solid circles are individual electronic measurements. Triangles are pre-discovery photographic measurements. Arrows are upper limits from all of these sources. The fourth panel shows *K*-band fluxes measured by UKIRT. The lower panel shows 15-GHz radio data from the Ryle Telescope (http://www.mrao.cam.ac.uk/~guy/J1118+480/J1118480.list). The last point is based on the average flux from 2000 August to November.

One such source, XTE J1118+480, was discovered by *RXTE* on 2000 March 29 at the galactic coordinates $(l, b) = (157.62^\circ, +62.32^\circ)$ (Remillard et al. 2000) as a weak (39 mCrab), slowly rising X-ray source, the post-analysis revealing an outburst in 2000 January, with a similar brightness. The outburst history of the source is shown in Fig. 1.

The optical counterpart of XTE J1118+480 in outburst was a 13th magnitude star, coincident with a 18.8-mag object in the USNO catalogue (Uemura et al. 2000). Its optical spectrum was typical of X-ray novae in outburst (Garcia et al. 2000). An infrared counterpart was rapidly identified thereafter (Chaty et al. 2000). Taking the X-ray and optical fluxes given above, it is clear that this system exhibits a very low X-ray to optical flux ratio of 5 (in f_ν, see Remillard et al. 2000; Uemura et al. 2000), compared with a typical value of 500 for SXTs in outburst (see e.g. Tanaka & Shibazaki 1996). A weak 4.1-h (0.170 82-d) photometric modulation was rapidly discovered (Cook et al. 2000), associated with the orbital period of the source, or possibly a superhump period (Uemura et al. 2000). XTE J1118+480 therefore exhibits the shortest orbital period among the black hole candidates. Wagner et al. (2001) took spectra of this source near quiescence and observed a period 0.5 per cent smaller than during the outburst. They suggested that this difference was due to the presence of superhump modulations during the outburst, later confirmed by Zurita et al. (2002). Flickering with an amplitude of ~0.4 mag, and also a quasi-periodic oscillation (QPO) at 10 s, was observed in the optical, in the UV (Haswell et al. 2000) and also in the X-ray range (Revnivtsev, Sunyaev & Borozdin 2000), with an evolving frequency (Wood et al. 2000). A faint radio counterpart was detected at 6.2 mJy, but no jet feature could be spatially resolved (see Fender et al. 2001). Optical observations of the source in quiescence led to the determination of a large value of the mass function, $f(M) = 5.9 \pm 0.4\ \mathrm{M}_\odot$, suggesting that the compact object is a black hole (McClintock et al. 2001a; Wagner et al. 2001).

The location of XTE J1118+480 at an unusually high galactic latitude ($b = +62^\circ$) in the direction to the Lockman Hole implies that there is a very low absorption along the line of sight of the source. Garcia et al. (2000) estimated $E(B-V) \sim 0.024$, leading to a column density of $N_H \sim 1.4 \times 10^{20}$ cm^{-2}. The column density has been estimated as $N_H \sim 0.75$–1×10^{20} cm^{-2} (Hynes et al. 2000), $N_H \sim 0.75$–1.15×10^{20} cm^{-2} (Esin et al. 2001), $N_H \sim 1$–1.3×10^{20} cm^{-2} (McClintock et al. 2001b), $N_H \sim 0.7$–1.5×10^{20} cm^{-2} (Frontera et al. 2001a), all nearly consistent with the mean value in the direction of the Lockman Hole (0.5–1.5×10^{20} cm^{-2}, see Hynes et al. 2000). From analysis of optical spectra, Dubus et al. (2001) derived $N_H \sim 1.77$–4.47×10^{20} cm^{-2}. As we see, the exact column density is still a matter of debate, and will be one of the points discussed in this paper. McClintock et al. (2001a) estimated a distance of 1.8 ± 0.6 kpc, consistent with the value of $\geqslant 1.5$ kpc derived by Uemura et al. (2000).

We triggered our multi-epoch multiwavelength override program with the *Hubble Space Telescope* (*HST*)/*RXTE*/UKIRT to obtain early observations of this system. We also requested Director's Discretionary *Extreme Ultraviolet Explorer* (*EUVE*) observations because of the low value of interstellar absorption, and obtained the first ultraviolet [extreme ultraviolet (EUV)] spectrum of an SXT (Hynes et al. 2000; Mauche et al. 2000). We therefore have unprecedented broad-band coverage, of more than 80 per cent of the electromagnetic spectrum from the radio ($\lambda = 21$cm) to the γ-rays (180 keV) [see the spectral energy distribution (SED) in Fig. 4 in Section 2.8]. The analysis of one of the epochs (corresponding in this paper to epoch 1, see Fig. 3 in Section 2.8) was described in Hynes et al. (2000) and we will briefly report here the main results (see also Esin et al. 2001 and McClintock et al. 2001b for an analysis of epoch 2). The corresponding SED suggested that the system was exhibiting a low-state mini-outburst, with the inner radius of the accretion disc estimated to be rather large, with a maximum value at $\sim 2000 R_s$ ($R_s = 2GM/c^2$; the Schwarzschild radius for an object of mass M) demanded by the EUV and X-ray data. One of the most striking features was the strong non-thermal (likely synchrotron) contribution in the optical and near-infrared (NIR) wavelengths, characteristic of outflows seen in jet sources. Indeed, the SED shows a very flat spectrum from the UV to the NIR (~1000–50 000 Å), suggesting that there is another source of NIR flux dominating any thermal disc emission, likely related to the radio emission, and therefore possibly of synchrotron origin.

We followed the evolution of this system from the outburst towards quiescence, to study the mechanisms underlying the outburst. Preliminary results were published in Chaty et al. (2001a,b). In this paper we will concentrate on the analysis and evolution of the SED. A companion paper (Hynes et al. 2003) discusses the multiwavelength variability properties. We describe the

multiwavelength observations in Section 2, present the results in Section 3, and discuss them in Section 4.

2 OBSERVATIONS

Observational details for our VLA, Ryle telescope, JCMT, UKIRT, *HST*, *EUVE*, *SAX*, *Chandra* and *RXTE* data follow.

2.1 Radio observations

All the radio (VLA, Ryle Telescope) and submillimetre (JCMT) observations are taken from references reported in Table 1.

2.2 NIR UKIRT observations

Near-infrared observations were carried out at the UKIRT 3.8-m telescope using UFTI (UKIRT Fast-Track Imager), IRCAM/TUFTI and also CGS4; some of which were already reported in Hynes et al. (2000). The log of the NIR observations is given in Table 2. The UFTI instrument is a cooled 1–2.5-μm camera with a 1024×1024 pixels^2 HgCdTe array. The plate scale is 0.091 arcsec pixel^{-1}, giving a field of view of 92 arcsec. The IRCAM/TUFTI instrument is a cooled 1–5-μm camera with a 256×256 pixels^2 InSb array. The plate scale is 0.081 arcsec pixel^{-1} with a field of view of 20.8 arcsec.

Images were taken through the wide-band filters J98 ($\lambda = 1.275$; $\Delta\lambda = 0.290$ μm), H98 ($\lambda = 1.670$; $\Delta\lambda = 0.280$ μm) and K98 ($\lambda = 2.205$; $\Delta\lambda = 0.41$ μm) with UFTI, and with all the above plus L′98 ($\lambda = 3.8$; $\Delta\lambda = 0.6$ μm) and M′98 ($\lambda = 4.675$; $\Delta\lambda = 0.250$ μm) with IRCAM/TUFTI.

The exposure times range between 10 and 60 s. The conditions were photometric. After taking each image of the object, an image of the sky was acquired, to allow subtraction of the blank sky. The images were further treated by removal of the dark current, the flat-field and the bright infrared sky. We also took a NIR *K*-band spectrum of this source using the CGS 4 instrument and a 0.6-arcsec slit on June 27.2 UT, which was featureless (see Chaty et al., in preparation).

2.3 Optical and ultraviolet *HST* observations

HST observations were performed with the Space Telescope Imaging Spectrograph (STIS; Leitherer et al. 2001) on the dates indicated in Table 3. These spanned the UV and optical bands at high and

Table 1. Log of radio observations. We tabulate here the epoch, date, Modified Julian Date, instrument and flux in mJy for every band.

Epoch	Date	MJD	Inst	1.4 GHz	8.3 GHz	15 GHz	23 GHz	350 GHz	Ref.
	30–31/03/00	51634	RT	–	–	6.2 ± 0.5	–	–	Pooley & Waldram (2000)
	31/03/00	51635	RT	–	–	7.8 ± 0.35	–	–	Dhawan et al. (2000)
1	02/04/00	51637	RT	–	–	7.5 ± 0.30	–	–	Dhawan et al. (2000)
1	03/04/00	51638	VLA	2.1 ± 0.1	6.0 ± 0.1	–	8.8 ± 0.3	–	Dhawan et al. (2000)
	05/04/00	51640	RT	–	–	8.7 ± 0.3	–	–	Fender et al. (2001)
2–6	16/03–25/06/00	51620–720	VLA	2.6 ± 0.4	6.5 ± 0.7	–	9.3 ± 1.2	–	Fender et al. (2001)
2–6	16/03–25/06/00	51620–720	RT	–	–	9.0 ± 1.0	–	–	Fender et al. (2001)
	08–11/00	51779–872	RT	–	–	0.15 ± 0.17	–	–	Pooley (private communication)
2–6	30–31/05/00	51695	JCMT	–	–	–	–	41 ± 4	Fender et al. (2001)
	09/09/00	51796	JCMT	–	–	–	–	<21	Fender et al. (2001)

Table 2. Log of the infrared observations. The epoch, date, MJD, instrument and magnitudes for every filter are reported. The magnitudes of the first epoch (corresponding to the detection of the infrared counterpart) were reported in Chaty et al. (2000), and those from Sternberg in Taranova & Shenavrin (2000). The observations of epochs 5 and 7 are reported in more details in Chaty et al. (in preparation).

Epoch	Date	MJD	Inst	*I*	*Z*	*J*	*H*	*K*	*L*′	*M*′
1	04/04/00	51638.2	UFTI			12.12 ± 0.02	11.75 ± 0.02	11.06 ± 0.02		
	12–15/04/00	51647.5	Sternberg			12.4 ± 0.2	11.9 ± 0.1	10.9 ± 0.1	9.2 ± 0.1	
2–4	18/04/00	51652.5	TUFTI			11.92 ± 0.07	11.43 ± 0.06	11.05 ± 0.08	9.71 ± 0.14	9.38 ± 0.42
	24/06/00	51719.2	UFTI					11.512 ± 0.004		
5	26/06/00	51721.2	CGS4					spectrum		
6	15/07/00	51740.2	UFTI					11.948 ± 0.006		
7	07/03/01	51975	UFTI	17.41 ± 0.05	17 ± 0.05	16.72 ± 0.05	16.15 ± 0.05	15.77 ± 0.05		

Table 3. Log of the optical and UV observations. The epoch, date, MJD, central wavelength and wavelength range are indicated, with in each case the exposure time in seconds.

Epoch	Date	MJD	E140M	E230M		G430L	G750L
	Central wavelength (Å):		1425	1978	2707	4300	7751
	Wavelength range (Å):		1123–1710	1574–2382	2303–3111	2900–5700	5236–10266
1	08/04/00	51642.7	9150	1300	1200	144	180
2	18/04/00	51652.6	3000	1000	700	1160	150
3	28/04/00	51663.3	1620	820	700	120	150
4	28/05/00	51692.8	1800	1000	750	120	204
5	24/06/00	51720.0	1750	1000	700	158	216
			3000				
6	08/07/00	51733.9	1700	950	750	120	224
7	28/09/00	51815	1250	2050	2050	400	407

Table 4. Log of the *EUVE* observations. The epoch, date, MJD and exposure time in seconds are indicated.

Epoch	Date	MJD	Exp. time
1	8–9/04/00	51642.603–51643.213	19 193.52
	13–14/04/00	51647.821–51648.430	19 553.9
2	16–19/04/00	51651.407–51654.102	80 200.1

Table 5. Log of the *SAX* observations. The epoch, date, MJD, energy bands and exposure time in seconds for the different instruments are indicated. For more details concerning the *SAX* observations see Frontera et al. (2001a).

Epoch	Date	MJD	LECS	MECS	HPGSPC	PDS
	Energy bands (keV):		0.12–4	1.7–10	7–29	15–200
2	14–15/04/00	51648–9	21197	29758	42138	20146

low resolution, respectively, using the E140M, E230M, G430L and G750L modes. For each visit, average calibrated spectra were extracted from standard *HST* pipeline data products. There was useful coverage from 1150 to 10 000 Å, although the region from 1195 to 1260 Å was completely dominated by Lyα absorption and N v emission (Haswell et al. 2002), so was excluded from our spectral energy distributions. On the dates where more than one observation of the same wavelength range was taken, the spectra were averaged to increase the signal-to-noise ratio. The documented absolute calibration accuracy is 5 per cent for the optical (CCD) modes and 8 per cent for the UV (MAMA) modes. The break between them is around 3100 Å, with some overlap. This systematic uncertainty is larger than any statistical uncertainties.

2.4 Extreme ultraviolet *EUVE* observations

EUVE observations of XTE J1118+480 took place during 2000 April 8.10–8.71, 13.32–13.93 and 16.91–19.60 UT. They are described in Hynes et al. (2000). The log of the *EUVE* observations is reported in Table 4. As in Hynes et al. (2000), we considered only the data between 70 and 120 Å, since longer wavelengths are heavily absorbed and dominated by noise. In the following plots showing data from *EUVE*, the vertical error bars are the 1σ errors from the photon statistics.

2.5 X-ray *SAX* observations

Beppo-SAX observed XTE J1118+480 four times, on 2000 April 14, May 4, June 26 and December 12. Here we show the observation taken on 2000 April 14–15, and reported in Table 5. The details of this observation can be found in Frontera et al. (2001a). Since these data were initially corrected with an interstellar absorption of 1.5×10^{20} cm^{-2}, we first uncorrected these data to obtain the observed flux, and then corrected them from the absorption with the desired value of N_H, as described in Section 3.1.

As shown in Fig. 2, although there is a good agreement between *SAX* and *Chandra* data in the interval $\log \nu = 16.6$–17.1 and between *SAX* and *RXTE* data for the interval $\log \nu = 18.5$–18.7, there is an inconsistency between the *SAX* and the *EUVE* observations for the interval $\log \nu = 16.5$–16.7 (probably due to the model used in fitting the *SAX* data combined with the low response of the detector at those wavelengths) and in the interval $\log \nu = 17.0$–18.5 between *SAX* and both *RXTE* and *Chandra* observations. This seems to be a calibration problem.

None the less, the *SAX* spectrum unambiguously shows the presence of a cut-off at an energy of $\log \nu \sim 19.5$, as discussed by Frontera et al. (2001a). Therefore, in the following we will include the *SAX* data only at high energies (in the interval $\log \nu = 18.8$–19.65)

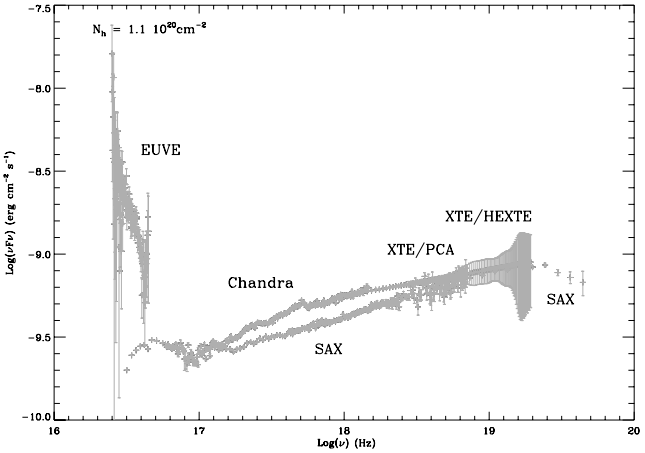

Figure 2. Comparison of epoch 2 SED as observed by the instruments *EUVE*, *Chandra*, *SAX* and *XTE*. The SED is corrected with $N_H = 1.10 \times 10^{20}$ cm^{-2}. This figure can be seen in colour in the on-line version of the journal on *Synergy*.

Table 6. Log of the *Chandra* observations. The epoch, date, MJD and exposure time in seconds are indicated. For more details about the *Chandra* observations see McClintock et al. (2001b).

Epoch	Date	MJD	Exp. time
2	18/04/00	51652.5	27200

2.6 X-ray *Chandra* observations

There was only one observation by *Chandra*, taken on 2000 April 18, reported in Table 6. Details are given in McClintock et al. (2001b). Since these data were corrected with an interstellar absorption of 1.3×10^{20} cm^{-2}, as for the *SAX* data, we first uncorrected these data to obtain the observed flux, and then corrected them for the absorption with the desired value of N_H, as described in Section 3.1.

2.7 X-ray *RXTE* observations and data analysis

We observed XTE J1118+480 with the *Rossi X-ray Timing Explorer (RXTE)* Proportional Counter Array (PCA) and High-Energy Timing Experiment (HEXTE) at five epochs selected to coincide with the *HST* visits. The log of the *RXTE* observations is reported in Table 7. The method used for the analysis of data is the same as that described in Hynes et al. (2000), therefore in the following we will just give the various parameters derived by analysing the different epochs.

Table 7. Log of the *RXTE* observations. We report here the epoch, date, MJD, exposure time in seconds for the PCA instrument and the observation ID.

Epoch	Date	MJD	Exp. time	Observation ID
1	08/04/00	51642.7	3900	50133-01-01-00
2	18/04/00	51652.6	4700	50133-01-02-00
3	28/04/00	51663.3	10 600	50133-01-03-00
4	28/05/00	51692.8	2400	50133-01-04-00
5	24/06/00	51720.0	5600	50133-01-05-00

Table 8. Log of the different epochs. The date and MJD are indicated. The '–' indicates that we used for the indicated epochs the observations of epoch 2, which is sensible since the SED did not change significantly in these wavelengths during 3 months.

Epoch	Date	MJD	Radio	UKIRT	*HST*	*EUVE*	*SAX*	*Chandra*	XTE	Colour
	log(ν)		9.0–11.6	13.78–14.48	14.47–15.41	16.38–16.61	16.61–19.68	16.76–18.23	17.78–19.68	
1	08/04/00	51642.7	x	x	x	x			x	Dark blue
2	18/04/00	51652.6	x	x	x	x	x	x	x	Light blue
3	28/04/00	51663.3	–	–	x				x	Dark green
4	28/05/00	51692.8	–	–	x				x	Light green
5	24/06/00	51720.0	–	x	x				x	Yellow
6	08/07/00	51733.9	–	x	x					Orange
7	09/00–03/01	51815–52467		x	x					Red

For the PCA, we used the 'standard mode' data (128 spectral channels, 16-s accumulations), selecting subintervals when the number of detectors on remained constant (∼90 per cent of the total time). We similarly extracted 256-channel spectral accumulations from the HEXTE science event (SE) data. A subset of PCA and HEXTE detector channels, corresponding typically to approximately 3–100 keV were used in our subsequent model fitting. Background rates for the PCA were estimated using the epoch-4 models, and response matrices were generated using the current calibration files and response-matrix generation software, all from the HEASOFT 5.1 release.

The source intensity was typically in the 30–40 mCrab range for each epoch, with typical PCA count rates of ∼80–120 count s^{-1} PCU^{-1} (source; the background is an additional 30 count s^{-1} PCU^{-1}). The spectra thus derived were found to be hard, with photon power-law indices of approximately 1.8 ± 0.1. A thermal Comptonization model (Sunyaev & Titarchuk 1980) with $\tau \simeq 3$ and $T_e \simeq 30$ keV, also provided acceptable fits (in either the power law or thermal Comptonization cases, a typical χ^2 per degree of freedom of the order of unity was obtained). There was no evidence (in terms of statistical improvement to our fits) for a soft-excess component, thus we conclude, as have others, that the source remained in the 'low/hard' spectral state throughout the outburst. In most cases, particularly 50133-01-03-00 for which the PCA exposure was approximately 10 000 s, there was a distinct positive residual corresponding to the 6.4-keV FeK resonance, thus a Gaussian line profile was included to refine the overall fit. The energy coverage was ∼3–26 keV with PCA and 11 to 207 keV with HEXTE. In all the figures we show only the data up to 80 keV (except for the first visit where we show them up to 120 keV), since at higher energies the noise dominates.

2.8 Broadband SED

For analysis, we separated the observations into the seven epochs reported in Tables 1–7. Table 8 summarizes the different facilities used at each epoch. For each epoch, observations in all bands are simultaneous or nearly simultaneous. The broad-band SEDs corresponding to all epochs are presented in Figs 3 and 4. In Fig. 3 they are shown with different normalizations for more clarity. We overplot all epochs in Fig. 4, and enlargements in radio, NIR–UV and EUV–X-ray regions are shown, respectively, in Figs 5–7. In all of these figures the data have been corrected with $N_H = 1.1 \times 10^{20}$ cm^{-2} corresponding to $A_v = 0.059$, as will be described in Section 3.1.

3 RESULTS

Before describing the results, in Section 3.1 we present the method used to correct for interstellar absorption.

3.1 Correction of interstellar absorption

The interstellar absorption was corrected in the following way. First, we choose a value for the column density by fitting the UV and EUV fluxes and slopes, as will be discussed in Section 3.5. For example, here we take $N_H = 1 \times 10^{20}$ cm^{-2}.

Using this value of column density, we then correct the *EUVE* data and *SAX* and *Chandra* X-ray data using the absorption cross-sections of Rumph, Bowyer & Vennes (1994) for H I, He I and He II with abundance ratios 1 : 0.1 : 0.01, typical of the diffuse interstellar medium.

Then, we assume that this inferred column density is interstellar, and we adopt an average gas-dust ratio of $\langle N(H_I + H_2)/E(B-V)\rangle = 5.8 \times 10^{21}$ cm^{-2} mag^{-1} (Bohlin, Savage & Drake 1978). This leads to the value of $E(B-V)$, equal to 0.017 in the example taken here. Taking the value of $R_v \equiv A_v/E(B-V) = 3.1$ typical of the diffuse interstellar medium (Cardelli, Clayton & Mathis 1989), we obtain the value of A_v (=0.053 here).

Finally, we correct the infrared (from UKIRT), optical and ultraviolet (*HST*) observations for interstellar absorption with the extinction law of Cardelli et al. (1989), using the derived value of absorption, leading to the inferred SED.

We note that even in the far-ultraviolet (FUV), reddening corrections are $\lesssim$15 per cent [depending on $E(B-V)$] and that the extinction curve and gas-to-dust scaling are not critical. Only in the EUV is the correction large.

3.2 Geometrical parameters of the system

We took a black hole mass of 7.2 ± 1.3 $M_\odot$ (McClintock et al. 2001a), which corresponds to a Schwarzschild radius of $R_s = 21$ km. The mass ratio has been measured as $Q = 1/q = M_1/M_2 = 27 \pm 5$ (an extreme value among SXTs, Orosz 2001), therefore the mass of the donor star $M_2 = 0.27 \pm 0.05$ $M_\odot$. The distance of the system has been determined as 1.71 ± 0.05 kpc (see the discussion in Section 3.3) and the orbital period to $P_{orb} = 0.169\,937(1)$ d $\sim$ 4.08 h (Zurita et al. 2002).

This gives an orbital separation $a = 1.76 \pm 0.1 \times 10^9$ m (Paczyński 1971). To derive the value of the outer radius of the accretion disc, we take the intermediate value between the tidal radius of the disc R_T and the 3:2 resonant radius R_{23}, since the source showed the presence of superhumps (see Section 1). The tidal radius of the disc is taken as 90 per cent of the Roche lobe radius, therefore $R_T/a = 0.58 \pm 0.01$ (Eggleton 1983) and the 3 : 2 resonant radius is $R_{23}/a \sim 0.47$ (Whitehurst & King 1991). Hence the outer radius we take is $r_{out} = 0.52a$. The inclination of the system is chosen to be $70^\circ \pm 10^\circ$, consistent with McClintock et al. (2001a, and also Zurita et al. 2002).

The inner radius of the accretion disc will be a free parameter, but will typically be between 300 and 450 R_s. This corresponds to a low

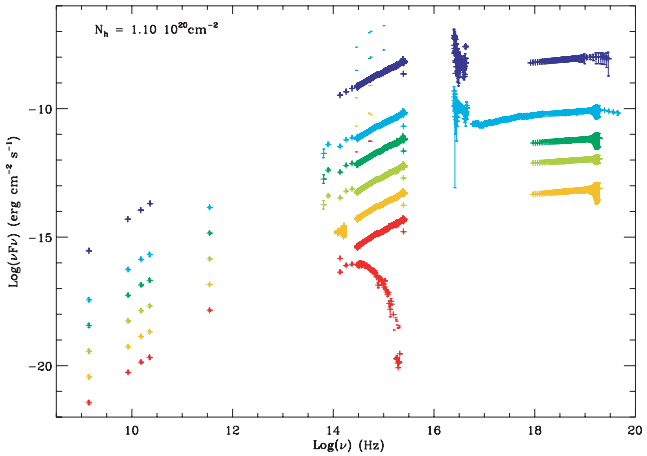

Figure 3. Spectral energy distributions of all the epochs, beginning from the top of the figure. Colour-codings are as given in Table 8. For easier reading, we multiplied epoch 1 by 10, and then divided epoch 2 by 10, epoch 3 by 100, epoch 4 by 10^3, epoch 5 and 7 by 10^4 and epoch 6 by 10^5.

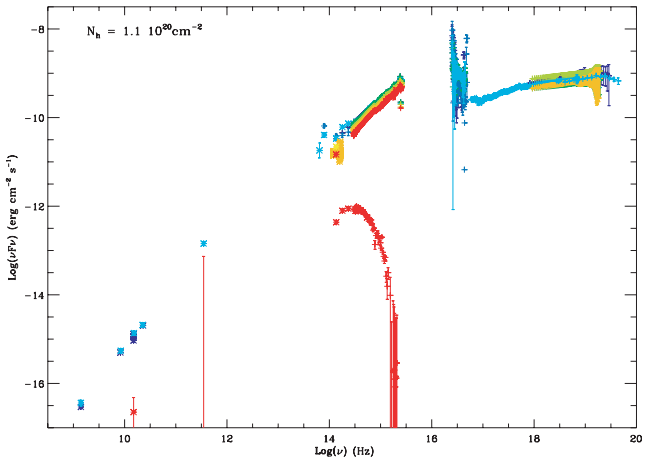

Figure 4. Spectral energy distribution for all the epochs overplotted.

state, in contrast to the high state where the accretion disc extends very close to the compact object, $r_{\rm in} \approx 3R_{\rm s}$, corresponding to the last stable orbit.

3.3 Fit to the nearly quiescent SED

To characterize the nearly quiescent system, we use only the epoch 7 data from UKIRT and *HST*. Since there is probably still some contamination from the accretion disc, we take the combination of two emission models, one representing the companion star and one representing the accretion disc. The spectral type of the companion star has been determined as K5–M1 V (McClintock et al. 2001a; Wagner et al. 2001). In our analysis, we therefore take an M1 V star photosphere ($T_{\rm eff}$ = 3400 K, Bessell, Castelli & Plez 1998). The radius of the mass donor star can be estimated with $R_2/a = 0.15 \pm 0.01$ (Eggleton 1983), therefore $R_2 = 0.39$ R$_\odot$. We take a blackbody model for the nearly quiescent accretion disc. We therefore fit the epoch 7 UKIRT and *HST* data with three free parameters: the fractional contribution of the secondary to the total emission, the temperature of the accretion disc, and the distance of the system. We found that the best-fitting parameters were a fractional contribution of 25 ± 2 per cent, a remnant accretion disc at 6000 ± 50 K and a

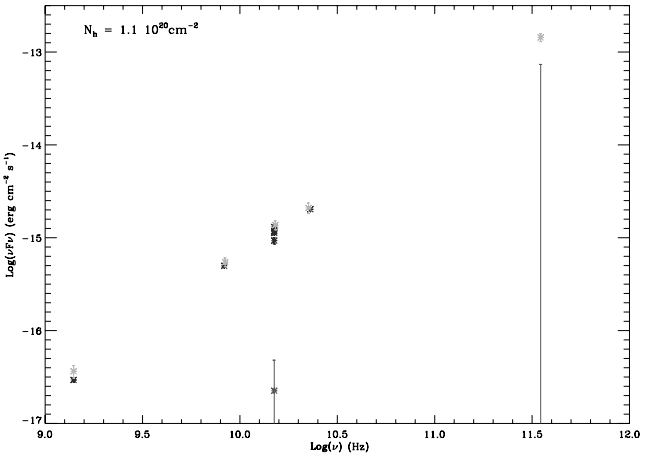

Figure 5. Radio SED for all the epochs. This figure can be seen in colour in the on-line version of the journal on *Synergy*.

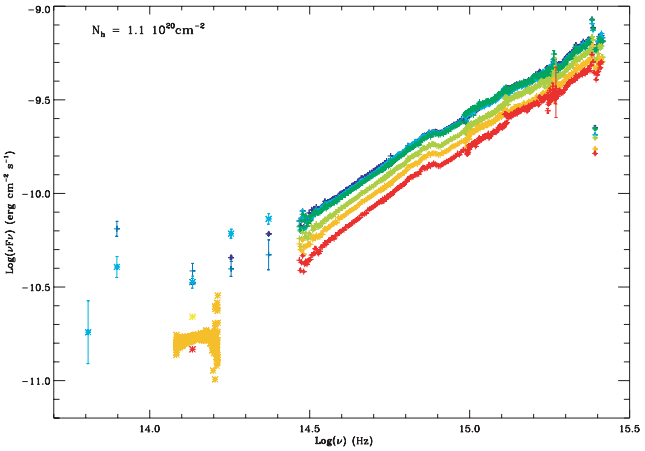

Figure 6. NIR-UV SED for all the epochs.

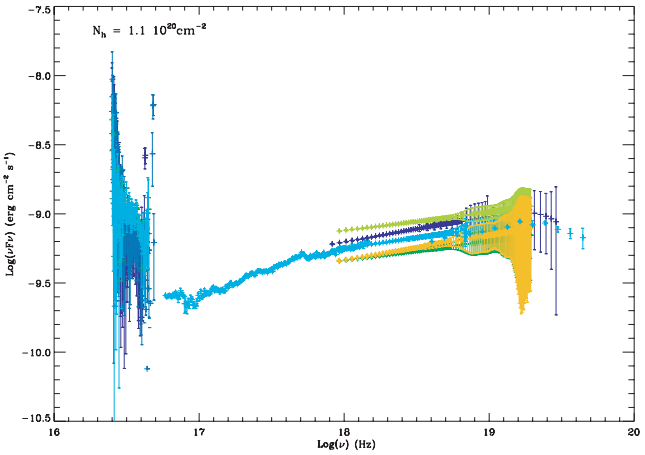

Figure 7. EUV-X SED for all the epochs.

distance of 1.71±0.05 kpc with a reduced $\chi^2 = 1.3$, and a tolerance of 10^{-5} (see Fig. 8). The fractional contribution of the secondary to the total emission which we derived is in agreement with the contribution of ∼28–36 per cent found by Wagner et al. (2001) and ∼34 ± 8 per cent by McClintock et al. (2001a) from optical spectroscopy. We also tried to replace the blackbody model by a power law, but the fit was worse, showing that the synchrotron contribution

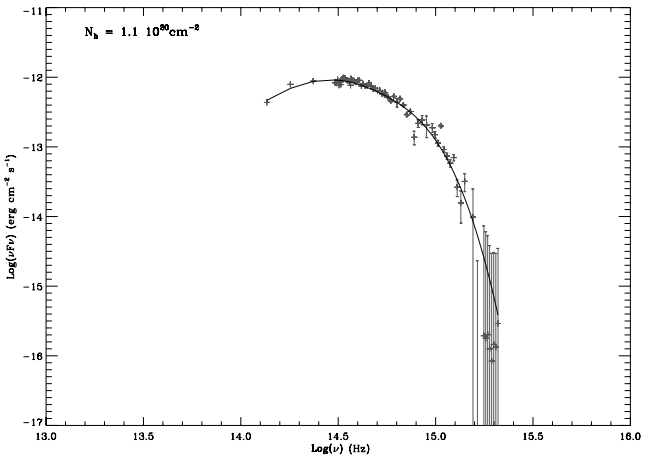

Figure 8. Fit of the epoch 7 (the nearly quiescent system), with a fractional contribution secondary/total emission of ∼25 per cent, a remnant accretion disc at ∼6000 K and a distance of ∼1.7 kpc, taking into account the emission of a M1V star at $T_{\rm eff} = 3400$ K with a radius $R_2 = 0.39\ {\rm R}_\odot$. This figure can be seen in colour in the on-line version of the journal on *Synergy*.

had decreased between epochs 1–6 and 7. We finally varied the absorption through the column density interval allowed by the broad-band SED (see Section 3.5) but this did not change the best-fitting parameters substantially. Therefore, our simple model gives a result consistent with the other methods, and in the following we will use the parameters derived from our analysis, to add the contribution from the companion star to the overall fits at other epochs.

It is interesting to point out that, by plotting the infrared colour magnitudes (observed on 2001 March, during the near-quiescence of the source, corresponding to epoch 7) on a Hertzsprung–Russell diagram, we derived that the companion star had a spectral type of M1 V (Chaty et al., in preparation), in agreement with the spectroscopic results. On the other hand, the radius of the companion star that we used for the fit in Fig. 8 is smaller than an isolated main-sequence star by a factor of 2. However, Haswell et al. (2002) showed that the companion star of XTE J1118+480 is an evolved star, consequently it may well have a different radius to an isolated main-sequence star of the same type.

3.4 Epoch 2

As we can see in Fig. 4 (which we will discuss in more detail in Section 3.8), there were no gross changes in the SED between epochs 1 and 6, so in the following we will consider the epoch where we have the most data, i.e. epoch 2. Our analysis differs from previous ones (see Section 1) because, in addition to the disc blackbody, we explicitly include contributions in different bands (for instance power-law spectra in radio, submillimetre–NIR and X-rays), together with the emission in the NIR–optical domain of the nearly quiescent system, using the results from Section 3.3. We are aware that this does not account for irradiation of the mass donor star, however, the fits are just intended to be illustrative. XTE J1118+480 is a unique source in term of its low absorption, allowing us to study its whole SED in great detail, derive some useful constraints and analyse the evolution from the outburst to near quiescence.

3.4.1 Model of the accretion disc

To fit the broad-band emission due to the accretion disc we use the simple parametrized model of Hynes et al. (2002). It is based on a combination of the classic viscously heated blackbody disc spectrum (Shakura & Sunyaev 1973; Frank, King & Raine 1992) and the modified temperature distribution for an irradiated disc (Cunningham 1976; Vrtilek et al. 1990). See these papers for derivations of the relevant temperature distributions, and Dubus et al. (1999) for a critique of the assumptions.

The model spectrum is calculated by summing a series of black bodies over radius. The local effective temperature of a disc annulus is determined by the emergent flux at that radius, such that $T_{\rm eff}^4 \propto F_{\rm bol}$. The emergent flux is the sum of viscous energy release within that annulus, $F_{\rm visc} \propto T_{\rm visc}^4$, and the X-rays reprocessed by the annulus, $F_{\rm irr} \propto T_{\rm irr}^4$. Hence the effective temperature contains contributions from viscous heating ($T \propto R^{-3/4}$) and irradiation ($T \propto R^{-3/7}$). The effective temperature profile of the disc is therefore represented by

$$T_{\rm eff}^4(R) = T_{\rm visc}^4(R) + T_{\rm irr}^4(R).$$

Both profiles are effectively controlled in the model by the temperature at the outer radius of the disc. The viscous temperature, $T_{\rm visc}(R_{\rm out})$, is a free parameter, typically around 7500 K; the irradiation temperature, $T_{\rm irr}(R_{\rm out})$, we usually take to be $T_{\rm irr}(R_{\rm out}) = 0$ K (but see Section 3.6).

The detailed fit is the sum of the secondary star (or nearly quiescent system), the model of the accretion disc in the low state, and three different power laws demanded by the data in the radio, NIR and X-ray bands, with respective spectral indices of 0.5, −0.15 and −0.8, taking the convention

$$f_\nu \propto \nu^\alpha. \quad (1)$$

As the figures show, these three power laws are natural fits to the SED. They have the respective expressions: $f_{\nu\rm radio} = 7 \times 10^{-31} \times \nu^{1/2}$ between 1×10^9 and 4×10^{11} Hz; $f_{\nu\rm nir} = 2.5 \times 10^{-23} \times \nu^{-0.15}$ between 4×10^{11} and 8×10^{14} Hz; and $f_{\nu\rm x} = 1.2 \times 10^{-13} \times \nu^{-0.8}$ between 8×10^{14} and $10^{19.3}$ Hz.

3.4.2 Examining the SED

We show epoch 2 with the different models and fit in Fig. 9. We clearly see two main characteristics. First, the source is exhibiting

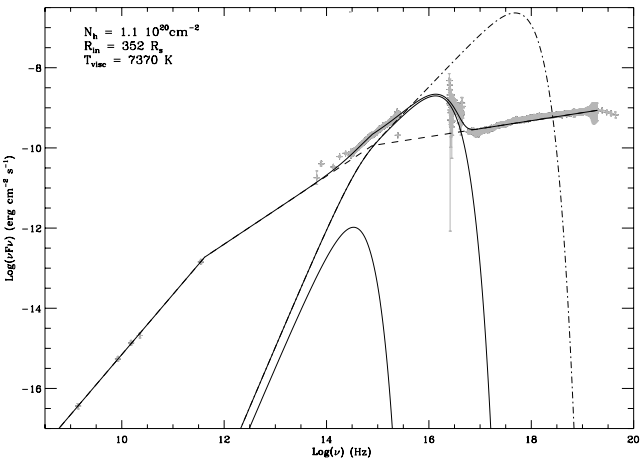

Figure 9. Spectral energy distribution for epoch 2 corrected with $N_H = 1.10 \times 10^{20}$ cm^{-2}. $R_{\rm in}$ and $T_{\rm visc}$ given in the figure are those derived by our fits. The lower solid thick curve is the emission representing the near-quiescent system, the intermediate solid thin curve is the multicolour blackbody disc in the low state, and the upper dash dot thin curve is the multicolour blackbody disc in the high state. The straight dashed lines are the three different power laws, as described in Section 3.4. The solid curve following the data is the sum of the contributions from the near-quiescent system, the accretion disc in the low state, and the three power laws. This figure can be seen in colour in the on-line version of the journal on *Synergy*.

Table 9. Results of different fits according to N_H. The N_H is fixed, $R_{\rm in}$ and $T_{\rm visc}$ are free parameters. Although it is not an independent parameter in the fits, we give $T_{\rm in}$ for information. The tolerance used in the fits was 1×10^{-2} (except where an asterisk is written, where the tolerance was between 0.1 and 1). Reasonable fits appear to be with N_H between 0.8 and 1.3×10^{20} cm^{-2}, and by inspecting the figures 1.1×10^{20} cm^{-2} seems to be the best value, and we will keep it for the rest of the paper (see the text for a discussion of this).

N_H ($\times 10^{20}$)	$R_{\rm in}$ ($R_{\rm s}$)	$T_{\rm visc}$ (K)	$T_{\rm in}$ (eV)	χ^2
0.70*	1369	7373	8.53	65
0.75*	970	7320	10.97	58
0.80	450	7246	19.32	54
0.85	427	7266	20.15	54
0.90	407	7286	20.94	54
0.95	389	7306	21.72	55
1.00	374	7327	22.44	55
1.05	362	7348	23.06	56
1.10	**352**	**7370**	**23.62**	**56**
1.15	354	7394	23.60	57
1.20	354	7418	23.67	57
1.25	356	7442	23.65	58
1.30	326	7460	25.27	58
1.35	310	7480	26.37	59
1.40	316	7505	26.08	60
1.45	313	7528	26.35	60
1.50	310	7551	26.62	61
1.55	307	7575	26.90	62
1.60	308	7599	26.92	62
1.65	306	7622	27.13	63
1.75	302	7669	27.57	65
1.90	296	7739	28.25	67
2.05	292	7810	28.80	70

a very low low/hard state (Hynes et al. 2000); secondly, there is a strong non-thermal contribution in the radio domain with an inverted spectrum, extending up to the UV wavelengths, and even in the X-rays. We will develop this later.

In most of our fits the typical values of the inner disc temperature, $T_{\rm in}$ are between 20 and 30 eV and those of the inner disc radius $R_{\rm in}$ are between 300 and $450R_{\rm s}$ (see Section 3.5 below and Table 9). These values are consistent with those derived by McClintock et al. (2001b), but the inner radii are higher than that derived by Esin et al. (2001), consistent with their model, including a significant advection-dominated accretion flow (ADAF) contribution to the EUV.

3.5 The hydrogen column density, $N_{\rm H}$

We now try to better constrain the value of N_H by fitting the whole SED corrected with different values of N_H, with the inner radius of the accretion disc and the outer temperature as free parameters. All the other parameters are taken as described in previous sections. The results are reported in Table 9. The best fits had a reduced χ^2 of 54, with 728 degrees of freedom. This high value of the reduced χ^2 just shows how illustrative the fits are, because detailed spectral features such as the Balmer jump and the dip in the *Chandra* spectrum are not fitted. From the χ^2 values obtained and inspection of corresponding figures, reasonable fits appear to be with N_H between 0.8 and 1.3×10^{20} cm^{-2}.

With $N_H = 1.45 \times 10^{20}$ cm^{-2} ($R_{\rm in} = 313R_{\rm s}$) no accretion disc models are simultaneously consistent with the very different slopes in the UV and the EUV. With $N_H = 0.75 \times 10^{20}$ ($R_{\rm in} = 970R_{\rm s}$) the presence of the X-ray power law makes it impossible to reconcile both high UV and low EUV fluxes. $N_H = 1.1 \times 10^{20}$ cm^{-2} is the only one of the values considered here which is consistent with both accretion disc models and the UV/EUV fluxes and slopes. We present the epoch 2 SED corrected with the column density $N_H = 1.1 \times 10^{20}$ cm^{-2} in Fig. 9.

Therefore, from the results of the fits, and also by plotting these results on the observations, $N_H = 0.8$–1.3×10^{20} cm^{-2} seems to be the preferred value. In the following we will consider the value of $N_H \sim 1.1 \times 10^{20}$ cm^{-2} as the most likely, and we will draw all the figures with this value.

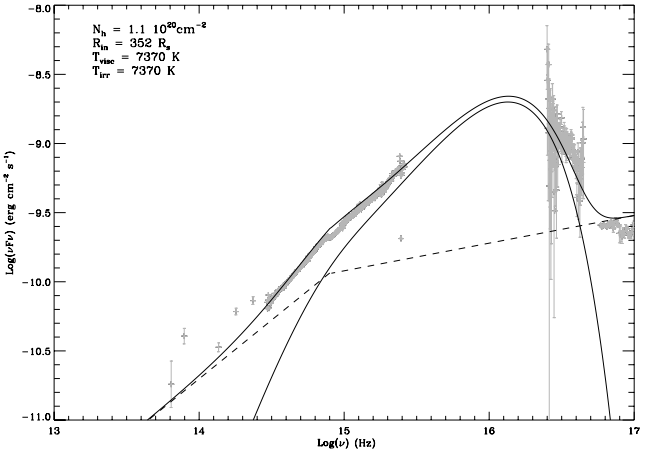

Figure 10. Spectral energy distribution for epoch 2 corrected with $N_H = 1.1 \times 10^{20}$ cm^{-2}, $R_{\rm in} = 352R_{\rm s}$ and with an irradiation of $T_{\rm irr}(R_{\rm out}) = 7370$ K (see Section 3.4.1). This figure can be seen in colour in the on-line version of the journal on *Synergy*.

3.6 Irradiation

In Fig. 10 we present the epoch 2 SED corrected with the column densities 1.10×10^{20} cm^{-2}, taking into account an irradiation with $T_{\rm irr}(R_{\rm out}) = 7370$ K, as described in Section 3.4.1. Fig. 9 shows the same SED without any irradiation. We can see that the slopes in the optical/UV parts of the spectrum are not consistent with the presence of irradiation. However, the irradiation component in our fit presents lots of assumptions, mainly concerning the geometry of the irradiating/irradiated region. Therefore, in view of the uncertainties in the irradiation function, although it is not required by our characterization of the data (which is also very crude), some irradiation of the disc cannot be ruled out.

3.7 Contributions to $L_{\rm bol}$

The luminosity due to thermal–viscous dissipation in the accretion disc is given by integrating the luminosity σT^4 between $R_{\rm in}$ and $R_{\rm out}$, for the two faces of the disc:

$$L_{\rm disc} = 2 \times 2\pi\sigma T_{\rm out}^4 R_{\rm out}^3 \left(\frac{1}{R_{\rm in}} - \frac{1}{R_{\rm out}} \right).$$

Adopting values typical of the fits in previous sections, i.e. $R_{\rm in} = 352R_{\rm s}$ (corresponding to $T_{\rm in} = 23.6$ eV) and $T_{\rm visc} = 7370$ K, we obtain $L_{\rm disc} = 2.2 \times 10^{36}$ erg s^{-1}.

In the three power laws corresponding, respectively, to the radio, NIR and X-ray domains, we integrate $F_\nu \propto \nu^\alpha$ in the frequency range given in Table 10, and multiply it by $4\pi D^2$ (i.e. assuming isotropic emission). The corresponding luminosities are given in Table 10. Therefore, assuming that $L_{\rm X-rays}$ is representative of the

Table 10. Contributions $L_{\rm bol}$ in different parts of the SED (called radio, NIR and X-rays following the convention given in Section 3.4.1). The frequency is given in $\log_{10}(\nu/{\rm Hz})$ and the luminosity in erg s^{-1}.

	Radio	NIR	X-rays
Frequency	[9–11.6]	[11.6–14.9]	[14.9–19.3]
Luminosity	4.6×10^{31}	5.3×10^{34}	1.5×10^{36}

contribution from the corona, we have $L_{\rm disc} \gtrsim L_{\rm corona}$, and we will discuss this result later in Section 4.3.1. This is consistent with the fact that in the case where all the gravitational power is dissipated in a static corona, nearly half of the coronal luminosity intercepts the disc and is reprocessed/reflected so $L_{\rm disc} \sim L_{\rm corona}/2$. Similarly if a fraction of the gravitational power is released in the disc (instead of the corona) $L_{\rm disc} \geqslant L_{\rm corona}/2$ (Haardt & Maraschi 1993).

3.8 The other epochs: evolution of the SED

There were no gross changes in the SED between epochs 1 and 6, so we overplot the fit to epoch 2 with the data from all epochs in Fig. 11. The SED did evolve a little during the outburst, and the best way to characterize this evolution is to quantify the change of the spectral index (defined as in equation 1) between optical ($10^{14.6}$ Hz) and X-ray (10^{18} Hz) domains. These domains are chosen because both show power-law spectra and we have simultaneous coverage during the six epochs of observations. This, reproduced in Fig. 12, shows that the electron energy distribution remains the same during the whole outburst. From Figs 5–7 it appears that the fluxes decrease slightly, however, the slopes do not change much. This suggests that the energy injected in the outflow decreases during the outburst.

We tried to reproduce this evolution of the SED by modifying some parameters of our simple model. One way to do this is by decreasing the outer (viscous) temperature. However, changing this temperature modifies the slope of the UV part of the SED, and as we can see in Fig. 6, this slope remains the same during the entire

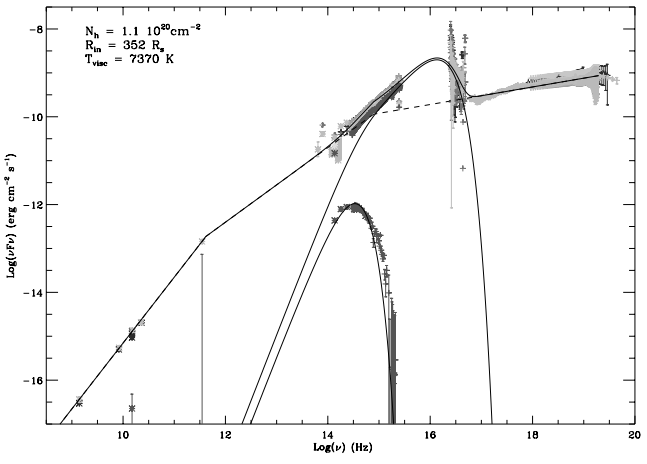

Figure 11. Spectral energy distribution: the fluxes are corrected with $N_H = 1.1 \times 10^{20}$ cm^{-2}. The overall fit is a multicolour blackbody disc model with an outer disc temperature of 7370 K and inner disc radius of $352R_{\rm s}$. Straight lines: different power laws, with spectral indices of 0.5, and -0.8 (similar to Hynes et al. 2000). The lower curve corresponds to the blackbody emission from the companion star. This figure can be seen in colour in the on-line version of the journal on *Synergy*.

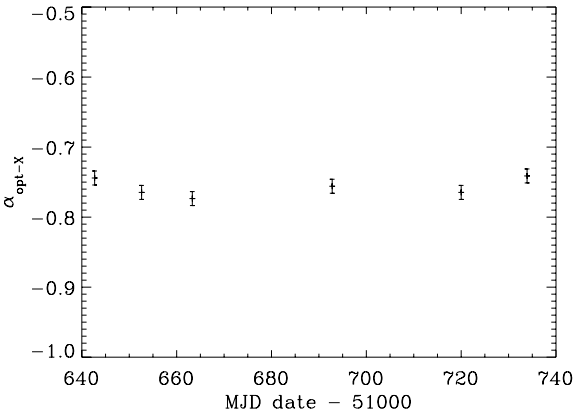

Figure 12. Evolution during the outburst of the spectral index linking the optical ($10^{14.6}$ Hz) and X-ray (10^{18} Hz) domains.

outburst. The other way to act on the multicolour blackbody disc would be to modify the inner radius, but this will only modify the EUV part of the SED. Therefore, the only way to reproduce this SED evolution is to act on the power laws, and we can indeed do this just by changing the constant of the power law (and not changing its exponent). This is consistent with a non-thermal contribution, which would have a decreasing energy during the outburst, but the same particle energy distribution. It is also suggestive of an outflow constrained to the central part of the accretion disc, the size of which would decrease during the outburst, which could be correlated with the increase in QPO frequency during the outburst (Wood et al. 2000).

This evolution is very interesting in the sense that it is different from what we see in other SXTs, and particularly in other states. For instance, in XTE J1859+226, Hynes et al. (2002) observed a change in the NIR–optical SED that they modelled as a change in viscous and irradiation temperature (as described in Section 3.4.1). In contrast, the evolution in XTE J1118+480 is mostly due to a change in the non-thermal (outflow) emission, compared with the thermal (disc) emission.

The lack of pronounced evolution of the SED during 3 months is also reminiscent of the behaviour of jet sources such as GRS 1915+105 and GX 339−4, in the so-called 'plateau state', where only small changes occur in the light curves. This, again, supports the idea of a steady outflow emanating from the source XTE J1118+480, as we will discuss in Section 4.2.

4 DISCUSSION

4.1 Variability and non-thermal contribution

A comprehensive discussion concerning the short time-scale variability of XTE J1118+480 during all the epochs of observations in the different wavebands (including NIR, UV and X-rays) can be found in Hynes et al. (2003). Here we just summarize the facts most relevant to our current analysis by combining our results on the SED and their results on the variability. Hynes et al. (2003) show that the XTE data exhibit a Poisson-subtracted fractional rms of approximately 35–37 per cent for the first observations decreasing to 26–28 per cent for the later ones. The UV variability is weaker than the optical or NIR, and stronger at longer wavelengths, with typical rms variability ∼3–4 per cent in the far-UV and ∼4–5 per cent in the near-UV. This suggests that at least some of the UV variability may be associated with the non-thermal component.

The ∼10-s QPO was seen in the optical, UV and X-rays, implying a common origin for this QPO throughout the spectrum. The sampling time of Hynes et al.'s (2003) NIR observations was insufficient to search for the QPO, however, they did detect flickering at NIR wavelengths, of larger amplitude (∼0.8 mag) than in the optical (∼0.4 mag). This NIR variability, up to 50 per cent, is consistent with a dominant non-thermal emission (Hynes et al. 2003). Furthermore, the featureless NIR spectrum we took in 2000 June (see data plotted in yellow in Fig. 3) is also consistent with the fact that the disc is not the only source of emission in this part of the spectrum (for more details concerning the NIR see Chaty et al. 2001b, in preparation). Hence both the SED and temporal behaviour suggest a strong non-thermal (probably synchrotron) emission at radio–UV wavelengths. Finally, it also shows that the cut-off frequency characteristic of the synchrotron radiation might be in the optical domain or even at higher frequencies.

4.2 How common is XTE J1118+480?

4.2.1 SED: comparison with other galactic sources

Several aspects of the broad-band spectrum of this source appear to be very similar to those of the other well-studied black hole binaries in the low state. The hard X-ray spectrum with a spectral index $\alpha \sim -0.8$ and a cut-off around 100 keV is typical of low/hard state spectra observed in Cygnus X-1 (e.g. Frontera et al. 2001b) or GX 339−4 (e.g. Zdziarski et al. 1998). The X-ray PDS spectrum of XTE J1118+480 is very similar to those of other black hole sources (Revnivtsev et al. 2000). However, the characteristic features are significantly shifted towards lower frequencies relative to other black hole sources with similar masses (cf. fig. 2 of Revnivtsev et al. 2000 and fig. 1 of Sunyaev & Revnivtsev 2000). This suggests that the X-ray-emitting region is larger in XTE J1118+480. Therefore, this hard X-ray variability, which is slower than in other SXTs, seems in turn to be consistent with a particularly large disc inner radius in this source. However, such 'slow and ubiquitous' QPOs have already been seen in other black hole candidates in the low state. For instance, QPOs at $P \sim 20$ s have been observed both in the X-ray and the optical bandes in the source GX 339−4 (Motch et al. 1983).

Another significant difference with other hard state sources is the low inner disc temperature inferred from our data. In the case of Cygnus X-1 in the hard state the inner temperature is $kT_{\rm in} \sim 150$ eV (see e.g. Balucinska-Church et al. 1995; Frontera et al. 2001b) contrasting with our derived value $kT_{\rm in} \sim 25$ eV (Table 9) for XTE J1118+480. This is consistent with a 'very low' low/hard state (Hynes et al. 2000). According to the multicolour blackbody disc model, this lower temperature implies a larger disc truncation radius than in typical sources (a few hundred $R_{\rm s}$ instead of a few tens). This can also simply be expressed in terms of $r_{\rm in}/r_{\rm out}$: this ratio is $4–7 \times 10^{-5}$ for a typical SXT such as XTE J1859+226, which we also observed with similar intensive coverage (Hynes et al. 2002). The $r_{\rm in}/r_{\rm out}$ ratio lies between 7×10^{-3} and 2×10^{-2} in the case of XTE J1118+480 (depending mainly on the value of the inner radius as derived with our fits). We also point out that the better energy coverage of the data available for XTE J1118+480 helped us to obtain accurate parameters, since the inner disc temperature of hard state sources is usually poorly determined due to strong interstellar absorption.

Finally, XTE J1118+480 differs from other transient sources by its exceptionally low X-ray to optical flux ratio (Tanaka & Shibazaki 1996) and its plateau-like light curve which contrasts with the exponential decay observed in many transients. However, once again in order to be consistent we have to compare XTE J1118+480 with other sources in the low/hard state, and when this is done it becomes less peculiar. For instance, the X-ray to optical flux ratio in the case of GX 339−4 can be as low as 2.5–3 (Motch et al. 1983), very similar to the value of 5 in the case of XTE J1118+480. Also, its plateau-like light curve is common in the jet source GRS 1915+105 (see e.g. Tanaka & Shibazaki 1996).

Therefore, the main difference with other sources is the prominence of the non-thermal contribution. Indeed, the radio–NIR spectrum presents an inverted spectrum, typical of non-thermal optically thick synchrotron emission. This combined with a lack of pronounced evolution of the SED strongly represents the signature of a jet. As a counterpoint, the radio spectral index during the 1999 outburst of XTE J1859+226 was negative most of the time, and the interval when it was positive was less than 4 d; its maximum value was 0.143 ± 0.180 (Brocksopp et al. 2002), cf. the steady 0.5 value in the 2000 outburst of XTE J1118+480. The radio–NIR component is much stronger in XTE J1118+480, exhibiting a low/hard state: in contrast the radio–NIR component was relatively weak in the high/soft state outburst of XTE J1859+226. This is consistent with the presence of an outflow (see e.g. Fender 2001).

This signature of a jet has been observed many times in GRS 1915+105 (see recent multiwavelength observations by Ueda et al. 2002), Cygnus X-1 (see Fender et al. 2000; Stirling et al. 2001) or GX 339−4 (Corbel et al. 2000). It is usually correlated with the appearance of the low/hard X-ray state spectrum, which is believed to be the result of a coupling between the Comptonizing corona and a compact jet (see, e.g., Corbel et al. 2000; Fender 2001). We will discuss this in more detail in Sections 4.2.2 and 4.3.2.

4.2.2 Comparison with galactic and extragalactic jet sources

The strong non-thermal contribution attributed to an outflow, implies that XTE J1118+480 is a *microquasar*. We therefore compare it with GRS 1915+105, the archetype of the microquasars. We can also compare the SED of XTE J1118+480 with typical SEDs of *quasars* given in Elvis et al. (1994), following the analysis of Ueda et al. (2002) in comparing GRS 1915+105 with typical quasars.

To compare the ratio of energy of the outflow with the accretion energy, we need estimates of both. The outflow energy can be estimated by taking the value νF_ν in the radio band ($\nu = 10^{10}$ Hz) for XTE J1118+480, GRS 1915+105 and quasars. However, for the measure of the accretion power, we have to take the wavelength where an optically thick thermal emission from the accretion disc presents a peak, therefore in the X-ray range ($\nu = 10^{18}$ Hz) in the case of GRS 1915+105, in the EUV ($\nu = 10^{16}$ Hz) in the case of XTE J1118+480 and in the UV ($\nu = 10^{15.2}$ Hz) in the case of quasars. Then we compare thereafter the ratio of νF_ν between the radio and X-rays for XTE J1118+480 and GRS 1915+105 with the ratio between radio and UV for quasars.

This outflow/accretion ratio is typically 10^{-6} for XTE J1118+480, when it is between 10^{-7} and 10^{-5} for GRS 1915+105, respectively, when this source is in a plateau state or exhibiting large radio flares. The value in XTE J1118+480 is intermediate between the two different values exhibited by GRS 1915+105. The main difference is that the ratio of XTE J1118+480 is stable, instead the ratio of GRS 1915+105 is varying on shorter time-scales between the two extreme values. This suggests that even if the contribution

of the outflow to the total energy budget in the two sources is comparable, there is a large difference in their behaviour, which is probably due to the fact that XTE J1118+480 is exhibiting a continuous outflow, and instead GRS 1915+105 shows energetic but sporadic ejections on short time-scales. Calculations of energy budget, taking into account different ejection behaviours are given in Chaty et al. (2001) by comparing GRS 1915+105 and SS 433.

For the quasars the outflow/accretion ratio is typically 10^{-2} and 10^{-6}, respectively, for radio-loud and radio-quiet quasars (Ueda et al. 2002). This suggests that XTE J1118+480 (and the microquasars) fall into the regime of radio-quiet quasars. The inverted radio spectrum resembles that of radio-quiet quasars, and the analogue of the millimetre break, around 10^{13} Hz, exhibited by the radio-quiet quasars and related to self-absorption, seems to be the submillimetre excess, around 10^{12} Hz, in XTE J1118+480. On the other hand, if the emission from the outflow also contributes substantially to the high-energy domain, then the outflow/accretion ratio becomes even bigger, up to the typical values of radio-loud quasars. If this analogy is real, then the intrinsic luminosity of the jet could dominate the energetics of XTE J1118+480, as in the case of the quasars (see Table 10).

Therefore, although the high-energy spectrum of XTE J1118+480 is very similar to what is observed in Seyfert galaxies, its phenomenology differs widely from that of strong extragalactic jet sources such as blazars. This is because blazars are dominated by relativistic beaming phenomena while the inclination in the case of XTE J1118+480 precludes this.

4.3 Accretion models

The low X-ray luminosity and the relatively large inner disc radius inferred from the comparisons with the multicolour blackbody disc model suggests that either the inner part of the accretion flow (i.e. at radii below $R_{\rm in}$) is radiatively inefficient [efficiency $L_{\rm bol}/(\dot{M}\times c^2) \sim 5\times10^{-4}$], or that a large fraction of material is ejected in an outflow, or both.

The ADAF model advocated by Ichimaru (1977) and Narayan & Yi (1994) explains low accretion efficiency as a consequence of the inner part of the flow advected into the black hole. The ADAF model was applied to XTE J1118+480 by Esin et al. (2001) who found a good fit to the optical–hard X-ray spectrum. Another possibility could be that the accretion power is advected into a jet or outflow, i.e. that a significant fraction of the energy could be used to power the jet. Indeed, ADAF solutions imply the flow is not bound (cf. Blandford & Begelman 1999). This outflow is indeed inferred from the flat radio spectrum and analogy with other sources in the hard state, where evidence for jets exists, as we discussed in Section 4.2. The most striking example of such sources is Cygnus X-1, which presents radio and X-ray spectra very similar to that of XTE J1118+480 and where a milliarcsec radio jet could be resolved (Stirling et al. 2001). However, since in XTE J1118+480 the fraction of the luminosity that can be firmly attributed to the jet represents only a few per cent of the total luminosity (see Section 3.7), the jet would have to be radiatively inefficient.

Actually the standard two-dimensional ADAF solution is likely to be strongly affected by the presence of the outflow and, more generally by the development of convective instabilities that only appear in two-dimensional solutions (see e.g. Stone, Pringle & Begelman 1999; Abramowicz, Lasota & Igumenshchev 2000; Igumenshchev, Abramowicz & Narayan 2000; Narayan, Igumenshchev & Abramowicz 2000; Quataert & Gruzinov 2000). As a consequence of the large theoretical uncertainties, we prefer to illustrate the possible presence of a hot optically thin geometrically thick component at the centre of the cold outer disc using a more phenomenological approach based on the constraints given by the observations and energy balance conditions as described below.

4.3.1 The hot disc model

We will now model the optical–hard X-ray spectrum, by assuming that the hot component comprises a sphere with radius equal to the cold disc truncation radius. The geometry is very similar to that of the sphere+disc geometry detailed in Dove et al. (1997).

To limit the number of parameters, and to avoid the uncertainties concerning the strength of the magnetic field, we further assume that the dominant cooling mechanism in the hot plasma is Compton cooling by the soft photons produced in the external disc. Other possible cooling mechanisms (bremsstrahlung, thermal synchrotron) are assumed to be negligible. This is a good approximation for luminous accreting black hole sources (Wardziński & Zdziarski 2000). In the case of XTE J1118+480, however, cyclotron/synchrotron and bremsstrahlung could be important cooling mechanisms (cf. Frontera et al. 2001a), but are not necessarily. We will discuss this further below, and will show how our assumption turns out to be consistent with the data.

We therefore used the non-linear Monte Carlo code of Malzac & Jourdain (2000) to compute the Comptonized spectrum emitted by the hot phase (the inner accretion flow) radiatively coupled in energy balance with the outer cold standard disc. In practice, we assume a homogeneous density, dissipation and heating rate inside the hot sphere. For a fixed Thomson optical depth, the hot plasma temperature is computed by balancing the heating and cooling. Possible temperature gradients due to the unavoidable inhomogeneity of the Compton cooling are accounted for by dividing the hot sphere into 10 homogeneous zones with equal volumes where the energy balance is computed locally. We neglect the effects of irradiation on the disc temperature profile, i.e. we assume the standard viscously heated multicolour blackbody disc ($T \propto R^{-3/4}$). The reprocessed emission is accounted for by re-emitting the absorbed energy, at the point it impinged on the external disc, with a blackbody spectrum at the local disc temperature.

The escaping X-ray spectrum is controlled mainly by the ratio of the volume-averaged dissipation rate in the hot phase (electron heating) to the soft flux from the disc that enters the cold phase (controlling the cooling). This ratio defining the energy balance of the hot component depends both on the assumed geometry and the fraction of radiated power dissipated in the hot phase:

$$f = L_{\rm c}/(L_{\rm v} + L_{\rm c}), \tag{2}$$

where $L_{\rm c}$ is the power radiated in the hot phase, $L_{\rm c} \sim L_{\rm X}$. $L_{\rm v}$ is the power viscously dissipated in the outer disc. The cold disc emission arises from both internal viscous dissipation $L_{\rm v}$, but also from reprocessing of the Comptonized hard X-rays irradiating the external disc. For our assumed geometry approximately one-third of the hard X-ray luminosity is intercepted by the disc. The observed disc luminosity is thus

$$L_{\rm disc} = [(1-f) + f/3](L_{\rm v} + L_{\rm c}) \tag{3}$$

and in the case of XTE J1118+480, f can be determined observationally

$$f \sim 1 \Big/ \left(\frac{2}{3} + \frac{L_{\rm disc}}{L_{\rm X}}\right) \sim 0.33. \tag{4}$$

The fraction of disc luminosity due to reprocessing is small, $\sim f/(3-2f) = 0.14$ and irradiation is unlikely to affect the outer disc structure. In particular, the local temperature depends only weakly on the total flux ($T \propto F^{1/4}$), thus for a local irradiating flux of 20 per cent of that of the local viscous flux, the disc temperature increases by less than 5 per cent. We note that this is perfectly in agreement with our observations, suggesting that effects of disc irradiation on the temperature profile should be weak (if any, see Section 3.6). Within the framework of the sphere+disc model, this 'weak irradiation' hypothesis is corroborated by the relatively low observed ratio of Comptonized to thermal emission. Therefore, our simple multicolour blackbody and power-law fits are consistent with our more sophisticated model assumptions. We also note that this geometry predicts an amplitude for the reflection component $R \sim 0.3$, which is slightly above the upper limits obtained by Frontera et al. (2001a) for their fits assuming low metallicity abundances in the disc (but see also Miller et al. 2002). However, even if such low-Z abundances might be related to a possible halo origin, as argued for by Wagner et al. (2001) and Mirabel et al. (2001), we point out that the metallicity should be higher than expected for a halo object, since the mass donor star is probably a CNO processed core (Haswell et al. 2002).

The spectral shape depends on five parameters: the disc outer temperature $T_{\rm out}$ and radius $R_{\rm out}$, the disc inner radius $R_{\rm in}$, and the fraction of accretion energy dissipated in the hot sphere to that dissipated in the accretion disc f, the hot sphere optical Thomson depth τ with respect to the sphere radius. The unique broad-band coverage in XTE J1118+480 constrains all the parameters relatively well.

In the simulation shown in Fig. 13 the cold disc parameters (and especially the locally emitted blackbody spectrum at its surface corresponding to the standard temperature dependence) have been set to values close to that assumed or derived from the fits of Section 3.4, namely $R_{\rm out} = 12 \times 10^3 R_{\rm s}$ (80 per cent of the Roche lobe radius), $R_{\rm in} = 300 R_{\rm s}$, $T_{\rm out} = 8000$ K. The Thomson optical depth along the sphere radius was fixed at $\tau = 1$ as indicated by the fit of Frontera et al. (2001a) for a spherical geometry, and $f = 0.33$ as discussed above. We did not include in the model any absorption as seen at $\log(\nu) \sim 17$, which was attributed to a warm absorber by Esin et al. (2001).

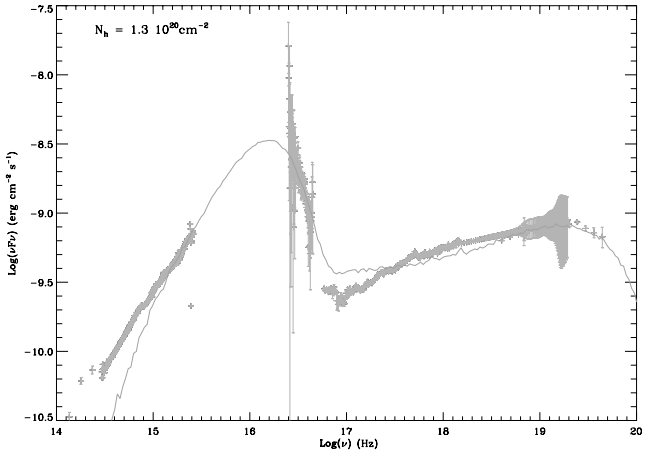

Figure 13. Modelling the optical to hard X-ray spectrum. The hot disc scheme is illustrated here, where we compare the non-linear Monte Carlo simulation for a central spherical hot plasma which radiates through Comptonization of the soft photons emitted by the outer cold disc both through internal viscous dissipation and reprocessing of the Comptonized hard X-rays (the latter being ≈20 per cent of the disc emission). See Section 3.1. This figure can be seen in colour in the on-line version of the journal on *Synergy*.

The most important parameters for the X-ray emission are f and $\tau . f$ controls the Compton y parameter of the plasma at equilibrium $y \propto \tau T_{\rm e}$ and thus the X-ray photon index Γ is very sensitive to f. With the f value independently provided by the observed luminosity of the cold and hot components, the model produces $\Gamma = 1.82$ (2–10 keV), in agreement with the results from spectral fits of the *SAX* data (Frontera et al. 2001a). Since all the parameters determining the X-ray slope are independently constrained, such an agreement is very remarkable. At fixed f, the parameter τ controls mainly the temperature of the hot phase. From energy balance we obtain a volume-averaged equilibrium temperature of the sphere of $kT_{\rm e} = 109$ keV in agreement with the value inferred from the fits of *SAX* data (Frontera et al. 2001a). Consequently, the shape of the high-energy cut-off is well reproduced.

Note that this model differs from the ADAF model of Esin et al. (2001) who considered cyclo-synchrotron radiation as the main source of soft photons for Comptonization and neglected the soft photons from the disc. We did precisely the opposite. In our model, if the bremsstrahlung and cyclo-synchrotron radiation were to constitute a significant additional source of soft photons, this would increase the cooling rate in the hot plasma, and, as a result we would obtain a much softer spectrum than was observed. The observations would then require a different geometry, reducing the soft photon input from the outer disc. For example, an oblate geometry for the central hot region could satisfy this requirement. In the extreme limit where the hot phase is geometrically thin along the disc axis we would be in the situation considered by Esin et al. (2001), dominated by cyclo-synchrotron radiation. Note that the correlated variability between the optical and X-rays suggests a causal connection, and that the synchrotron radiation emanating from the same region that produces the X-rays can contribute in the optical band (Merloni, Di Matteo & Fabian 2000), but not necessarily as a significant source of soft cooling photons. Therefore, this process is not inconsistent with our model where we neglected the synchrotron emission.

4.3.2 Jet corona models

If the X-ray emission is produced in the central part of the accretion flow, the ∼0.1 Hz QPO observed both in the X-ray and optical is difficult to explain (Merloni et al. 2000). On the other hand, it may be explained simply by a flux modulation at the Kepler frequency of the disc at $R_{\rm in}$. This suggests that a non-negligible fraction of the flux would be produced in a transition region where both the hot plasma and cold thin disc coexist.

This transition region could consist of a hot corona atop the external disc. The generation of magnetic field in the disc through magnetorotational instability and the subsequent buoyancy of the magnetic field (Tout & Pringle 1992; Miller & Stone 2000) is generally invoked as an efficient mechanism for the transfer of magnetic energy from the disc to a corona where it is dissipated through magnetic flares. This scenario for energy dissipation in the corona was built to explain a strong coronal emission in the innermost part of the accretion flow. At the large distances we infer for the disc truncation radius, it is expected to be less efficient.

Therefore, if $R_{\rm in}$ is as large as we infer, alternative dissipation processes such as transport and heating through Alfvén waves (Tagger & Pellat 1999) or viscous dissipation in a fast accreting corona (Różańska & Czerny 2000) may appear preferable. Actually, if the inner flow was very inefficient (or even non-existent), the X-ray

emission could be fully dominated by the coronal emission. In this context, mildly relativistic ejections of coronal plasma are likely to be important in hard state sources (Beloborodov 1999; Malzac, Beloborodov & Poutanen 2001). In particular, it may explain the relatively hard X-ray spectrum and absence of reflection observed in XTE J1118+480 together with being consistent with the presence of an outflow. From the theoretical side relativistic outflow models often require an accretion disc corona as the place where the flow is initially powered (see Tagger & Pellat 1999; Merloni & Fabian 2001). The accretion disc corona picture would thus be physically compatible with the presence of a jet inferred from the flat radio spectrum.

In accretion disc corona models a substantial part of the disc emission is due to reprocessing of the hard X-rays impinging on the disc. As the optical, near-UV and far-UV variability indicates that reprocessing is weaker than the extremely strong synchrotron component (Hynes et al. 2003), this constrains the corona to be active only in the innermost part of the disc. The X-ray luminosity should then come from a region of the disc forming a thin ring with inner radius $R_{\rm in}$ and outer radius $R_{\rm c}$.

One can obtain an estimate of $R_{\rm c}$ by assuming that at distances lower than $R_{\rm c}$, all the accretion power goes to the corona while at larger distance it is dissipated viscously in the disc. Since the estimated X-ray luminosity is approximately half of that of the disc and approximately half of the coronal emission is intercepted by the disc, we can conclude that approximately half of the disc luminosity could be due to the reprocessing. Assuming that the reprocessed luminosity is half of that of the disc one obtains $r_{\rm c} \sim 2R_{\rm in}$.

We point out that our results are perfectly consistent with the accretion–ejection instability (AEI) model (Tagger & Pellat 1999), which predicts that Alfvén waves efficiently power the corona and the jet in a range of distance comprised between $R_{\rm in}$ and the corotation radius of the Rossby vortex at a few $R_{\rm in}$ (Varnière & Tagger 2002). Particularly, from the value of the inner radius that we derive with our fits, the AEI predicts a QPO which is well in agreement (Varnière, Rodriguez & Tagger 2002) with the values observed in UV, optical and X-rays during the outburst at Fourier frequencies $\sim$0.1 Hz. The prediction on the QPO frequency evolution would also be consistent with the observations by Wood et al. (2000). The AEI context, by assuming equipartition between magnetic field and gas pressure, would exclude a Schwarzschild black hole, and favour a Kerr black hole rotating at a spin between 0.90 and 0.99 (P. Varnière, private communication). This QPO may be explained simply by a flux modulation due to the Keplerian rotation of the disc or, in the Tagger & Pellat (1999) framework, the presence of the spiral wave (P. Varnière, private communication).

We also note that in addition to the Comptonized emission from the hot disc and/or corona, a synchrotron component from the jet could also contribute in the X-rays. Such a non-thermal component was seemingly detected in GRS 1915+105 in a low/hard state (Vadawale, Rao & Chakrabarti 2001). In fact, the whole X-ray emission could even arise from pure synchrotron from the jet as demonstrated by Markoff, Falcke & Fender (2001). This model attributes all the X-ray luminosity of XTE J1118+480 to synchrotron emission from the jet. A potential problem for this model is that it predicts essentially no reflection component. This makes it difficult to transpose to other similar jet sources such as Cygnus X-1, where a significant reflection component is clearly observed and correlated with other X-ray spectral characteristics such as the photon index (Gilfanov, Churazov & Revnivtsev 1999). However, the pure synchrotron model cannot be formally ruled out, and we could also have both mechanisms acting at the same time.

5 CONCLUSIONS

We reported multiwavelength observations of XTE J1118+480 during its outburst, assembling the most complete spectral energy distribution of this source yet published, including our observations with UKIRT, *HST*, *RXTE*, *EUVE*, and adding observations from the literature: Ryle Telescope, VLA, JCMT, *Chandra* and *SAX*. We followed the source for 6 months, and show its evolution during the outburst. The main results of our broad-band multi-epoch coverage are given below.

(i) The source XTE J1118+480 was in a very low state throughout the outburst (estimated inner radius at $350R_{\rm s}$).

(ii) The column density is low, between 0.80 and 1.30 $\times$ 10^{20} cm^{-2}.

(iii) The accretion disc seems to be heated mainly by viscosity throughout the outburst, without a strong irradiation contribution.

(iv) It exhibited an inverted spectrum from radio to at least optical wavelengths, characteristic of a strong non-thermal (likely synchrotron) contribution, usually attributed to an outflow.

(v) By examining the near-quiescent system we found that the best-fitting parameters were a fractional mass donor star contribution of 25 ± 2 per cent, a remnant accretion disc at 6000 ± 50 K and a distance of 1.71 ± 0.05 kpc.

(vi) The quasi-absence of variation of the SED during 3 months is consistent with a steady outflow emanating from the source, similarly to other 'microquasars' in the 'plateau' state.

(vii) The ratio between radio and EUV energy, indicative of the outflow to accretion energy ratio, suggests that the source falls into the regime of radio-quiet quasars, and is also consistent with a steady outflow.

(viii) The small change of the SED in the optical–UV part, along with the constant power-law slopes during the whole outburst, is consistent with a continuous, gradual decrease of the outflow energy.

(ix) We modelled the emission from the optical to the hard X-rays with a hot disc model, showing that the high-energy part of the spectrum can emanate from the accretion flow. We therefore have to take into account the possibility that the high-energy emission from this source comes from (a) Comptonization, (b) pure synchrotron or (c) a mixture of both.

Although this object exhibits peculiar characteristics, e.g. a large inner disc radius and a likely origin in the halo, some of its characteristics are very similar to other sources, particularly in the low–hard state and exhibiting jets or outflows. This object is particularly important because its very low absorption reveals phenomena that until now were difficult to study. XTE J1118+480 facilitates testing and refinement of models for variability and emission in black hole accretors.

ACKNOWLEDGMENTS

We thank Christopher W. Mauche for fruitful discussions concerning absorption in the EUV, and for giving us the *EUVE* data. We are grateful to Mike Garcia for useful discussions concerning the evolution of the SED, to him and Jeff McClintock for giving us the *Chandra* data, and to Filippo Frontera for the *SAX* data. We thank Tom R. Geballe who obtained the NIR spectrum of XTE J1118+480 on 2000 June 26. We thank Guy Pooley for the Ryle Telescope data also used in this figure, and VSNET for all their alerts on XTE J1118+480 and their optical data used in Fig. 1. SC and JM thank Michel Tagger, Peggy Varnière and Josep Martí. SC, CAH and RIH

gratefully acknowledge support from grant F/00–180/A from the Leverhulme Trust. SC and JM acknowledge a travel grant from the Groupe de Recherche *Phénomènes Cosmiques de Haute Énergie* of the French Centre National de la Recherche Scientifique. JM acknowledges a grant from the European Commission (contract number ERBFMRX-CT98-0195, TMR network 'Accretion on to black holes, compact stars and protostars'). WC also acknowledges support from HST-GO-08647.10-A.

The United Kingdom Infrared Telescope is operated by the Joint Astronomy Centre on behalf of the UK Particle Physics and Astronomy Research Council. UKIRT Service observations of XTE J1118+480 through the year 2000 were obtained thanks to override time which was pre-approved in the case of outbursting transients (U/00A/45, PI SC), to be coordinated with our *HST* and *RXTE* observations. SC is grateful to the UKIRT staff for these override service observations, and in particular to Andy Adamson, John K. Davies, Sandy K. Leggett and Chris Davis.

Based on observations made with NASA/ESA *HST*, associated with proposal GO 8647. Support was provided by NASA through a grant from the Space Telescope Science Institute, which is operated by the Association of Universities for Research in Astronomy, Inc, under NASA contract NAS 5-26555. We finally thank the *HST/STScI* and *RXTE* support staff for ongoing efficient effort in these multi-epoch campaigns. This research has made use of NASA's Astrophysics Data System Bibliographic Services and quick-look results provided by the ASM/RXTE team.

REFERENCES

Abramowicz M.A., Lasota J., Igumenshchev I.V., 2000, MNRAS, 314, 775
Balucinska-Church M., Belloni T., Church M.J., Hasinger G., 1995, A&A, 302, L5
Beloborodov A.M., 1999, MNRAS, 305, 181
Bessell M.S., Castelli F., Plez B., 1998, A&A, 333, 231
Blandford R.D., Begelman M.C., 1999, MNRAS, 303, L1
Bohlin R.C., Savage B.D., Drake J.F., 1978, ApJ, 224, 132
Brocksopp C. et al., 2002, MNRAS, 331, 765
Cardelli J.A., Clayton G.C., Mathis J.S., 1989, ApJ, 345, 245
Charles P., 1998, in Abramowicz M.A., Bjomsson G., Pringle J.E., eds, Theory of Black Hole Accretion Disks 'Black Holes in our Galaxy: Observations'. Cambridge Univ. Press, Cambridge, p. 1
Chaty S., Haswell C.A., Smith G.P., Smail I., Hynes R.I., 2000, IAU Circ., 7394, 3
Chaty S., Haswell C., Hynes R., Shrader C., Cui W., 2001a, in Combes F., Barret D., Thévenin F., eds, SF2A-2001: Semaine de l'Astrophysique Francaise. EdP-Sciences, p. 349 (astro-ph/0108242)
Chaty S., Haswell C., Hynes R., Shrader C., Cui W., 2001b, in Gimenez A., Reglero V., Winkler C., eds, Proc. 4th INTEGRAL workshop. ESA Publications, Noordwijk, p. 491 (astro-ph/0102103)
Chaty S., Rodríguez L.F., Mirabel I.F., Geballe T., Fuchs Y., 2001, A&A, 366, 1041
Cook L., Patterson J., Buczynski D., Fried R., 2000, IAU Circ., 7397, 2
Corbel S., Fender R.P., Tzioumis A.K., Nowak M., McIntyre V., Durouchoux P., Sood R., 2000, A&A, 359, 251
Cunningham C., 1976, ApJ, 208, 534
Dhawan V., Pooley G.G., Ogley R.N., Mirabel I.F., 2000, IAU Circ., 7395, 2
Dove J.B., Wilms J., Maisack M., Begelman M.C., 1997, ApJ, 487, 759
Dubus G., Lasota J., Hameury J., Charles P., 1999, MNRAS, 303, 139
Dubus G., Kim R.S.J., Menou K., Szkody P., Bowen D.V., 2001, ApJ, 553, 307
Eggleton P.P., 1983, ApJ, 268, 368
Elvis M. et al., 1994, ApJS, 95, 1
Esin A.A., McClintock J.E., Drake J.J., Garcia M.R., Haswell C.A., Hynes R.I., Muno M.P., 2001, ApJ, 555, 483
Fender R.P., 2001, MNRAS, 322, 31
Fender R.P., Pooley G.G., Durouchoux P., Tilanus R.P.J., Brocksopp C., 2000, MNRAS, 312, 853
Fender R.P., Hjellming R.M., Tilanus R.P.J., Pooley G.G., Deane J.R., Ogley R.N., Spencer R.E., 2001, MNRAS, 322, L23
Frank J., King A., Raine D., 1992, Accretion Power in Astrophysics. Cambridge Univ. Press, Cambridge
Frontera F. et al., 2001a, ApJ, 561, 1006
Frontera F. et al., 2001b, ApJ, 546, 1027
Garcia M., Brown W., Pahre M., McClintock J., Callanan P., Garnavich P., 2000, IAU Circ., 7392, 2
Gilfanov M., Churazov E., Revnivtsev M., 1999, A&A, 352, 182
Haardt F., Maraschi L., 1993, ApJ, 413, 507
Haswell C.A., Skillman D., Patterson J., Hynes R.I., Cui W., 2000, IAU Circ., 7427, 1
Haswell C.A., Hynes R.I., King A.R., Schenker K., 2002, MNRAS, 332, 928
Hynes R., Mauche C., Haswell C., Shrader C., Cui W., Chaty S., 2000, ApJ, 539, L37
Hynes R.I., Haswell C.A., Chaty S., Shrader C.R., Cui W., 2002, MNRAS, 331, 169
Hynes R.I. et al., 2003, MNRAS, 345, 292
Ichimaru S., 1977, ApJ, 214, 840
Igumenshchev I.V., Abramowicz M.A., Narayan R., 2000, ApJ, 537, L27
Leitherer C. et al., 2001, STIS Instrument Handbook, Version 5.0. STScI, Baltimore
McClintock J.E., Garcia M.R., Caldwell N., Falco E.E., Garnavich P.M., Zhao P., 2001a, ApJ, 551, L147
McClintock J.E. et al., 2001b, ApJ, 555, 477
Malzac J., Jourdain E., 2000, A&A, 359, 843
Malzac J., Beloborodov A.M., Poutanen J., 2001, MNRAS, 326, 417
Markoff S., Falcke H., Fender R., 2001, A&A, 372, L25
Mauche C., Hynes R., Charles P., Haswell C., 2000, IAU Circ., 7401, 2
Merloni A., Fabian A.C., 2001, MNRAS, 332, 165
Merloni A., Di Matteo T., Fabian A.C., 2000, MNRAS, 318, L15
Miller K.A., Stone J.M., 2000, ApJ, 534, 398
Miller J., Ballantyne D.R., Fabian A.C., Lewin W.H.G., 2002, MNRAS, 335, 865
Mirabel I.F., Dhawan V., Mignani R.P., Rodrigues I., Guglielmetti F., 2001, Nat, 413, 139
Motch C., Ricketts M.J., Page C.G., Ilovaisky S.A., Chevalier C., 1983, A&A, 119, 171
Narayan R., Yi I., 1994, ApJ, 428, L13
Narayan R., Igumenshchev I.V., Abramowicz M.A., 2000, ApJ, 539, 798
Orosz J.A., 2001, The Astronomer's Telegram, 67, 1
Paczyński B., 1971, ARA&A, 9, 183
Pooley G.G., Waldram E.M., 2000, IAU Circ., 7390, 2
Quataert E., Gruzinov A., 2000, ApJ, 539, 809
Remillard R., Morgan E., Smith D., Smith E., 2000, IAU Circ., 7389, 2
Revnivtsev M., Sunyaev R., Borozdin K., 2000, A&A, 361, L37
Różańska A., Czerny B., 2000, A&A, 360, 1170
Rumph T., Bowyer S., Vennes S., 1994, AJ, 107, 2108
Shakura N.I., Sunyaev R.A., 1973, A&A, 24, 337
Stirling A.M., Spencer R.E., de la Force C.J., Garrett M.A., Fender R.P., Ogley R.N., 2001, MNRAS, 327, 1273
Stone J.M., Pringle J.E., Begelman M.C., 1999, MNRAS, 310, 1002
Sunyaev R., Revnivtsev M., 2000, A&A, 358, 617
Sunyaev R.A., Titarchuk L.G., 1980, A&A, 86, 121
Tagger M., Pellat R., 1999, A&A, 349, 1003
Tanaka Y., Shibazaki N., 1996, Annu. Rev. A&A, 34, 607
Taranova O., Shenavrin V., 2000, IAU Circ., 7407, 2
Tout C.A., Pringle J.E., 1992, MNRAS, 259, 604
Ueda Y. et al., 2002, ApJ, 571, 918
Uemura M. et al., 2000, Publ. Astron. Soc. Japan, 52, L15

Vadawale S.V., Rao A.R., Chakrabarti S.K., 2001, A&A, 372, 793
Varnière P., Tagger M., 2002, A&A, 394, 329
Varnière P., Rodriguez J., Tagger M., 2002, A&A, 387, 497
Vrtilek S.D., Raymond J.C., Garcia M.R., Verbunt F., Hasinger G., Kurster M., 1990, A&A, 235, 162
Wagner R.M., Foltz C.B., Shahbaz T., Casares J., Charles P.A., Starrfield S.G., Hewett P., 2001, ApJ, 556, 42
Wardziński G., Zdziarski A.A., 2000, MNRAS, 314, 183
Whitehurst R., King A., 1991, MNRAS, 249, 25
Wood K.S. et al., 2000, ApJ, 544, L45
Zdziarski A.A., Poutanen J., Mikolajewska J., Gierlinski M., Ebisawa K., Johnson W.N., 1998, MNRAS, 301, 435
Zurita C. et al., 2002, MNRAS, 333, 791

This paper has been typeset from a TEX/LATEX file prepared by the author.